Tracing field lines that are reconnecting, or expanding, or both

Jiong Qiu*

Department of Physics, Montana State University, Bozeman, MT, United States

The explosive release of energy in the solar atmosphere is driven magnetically, but the mechanisms that trigger the onset of the eruption remain controversial. In the case of flares and coronal mass ejections (CMEs), ideal or non-ideal instabilities usually occur in the corona, but it is difficult to obtain direct observations and diagnostics there. To overcome this difficulty, we analyze observational signatures in the upper chromosphere or transition region, particularly brightening and dimming at the base of coronal magnetic structures. In this paper, we examine the time evolution of spatially resolved light curves in two eruptive flares and identify a variety of tempo-spatial sequences of brightening and dimming, such as dimming followed by brightening and dimming preceded by brightening. These brightening−dimming sequences are indicative of the configuration of energy release in the form of plasma heating or bulk motion. We demonstrate the potential of using these analyses to diagnose the properties of magnetic reconnection and plasma expansion in the corona during the early stages of the eruption.

1 Introduction

It is well known that explosive energy releases in the form of solar flares and coronal mass ejections (CMEs) are driven magnetically. In this process, magnetic energy is converted to the kinetic energy of particles and the heat and bulk motion of plasmas (Thompson et al., 2021). CMEs open up a portion of the solar corona, along which energetic particles are released into interplanetary space and can impact the space weather. At present, routine measurements of the full disk magnetic field are available only in the lower solar atmosphere, the photosphere. Therefore, the capability to identify the solar surface signatures of an open magnetic structure and track magnetic field evolution prior to eruption will help us explore mechanisms governing the onset of the eruption and predict space weather.

Traditionally, coronal holes (Cranmer, 2009), or regions of persistent lack of emission at soft X-ray (SXR) and extreme ultraviolet (EUV) wavelengths, are considered to map the feet of open field lines on the solar surface. The lifetimes of coronal holes range from many days to multiple weeks (Lowder et al., 2017, and references therein). The temporary, and often abrupt, opening up of the magnetic structure associated with a CME produces transient coronal holes, also called coronal dimmings (Sterling and Hudson, 1997). A comprehensive review of observational signatures and an interpretation of coronal dimmings has been

provided by Veronig et al. (2024, in press). Mechanisms causing the explosive "opening up" of the corona include the onset of an ideal instability, in which the global force balance is lost during the quasi-equilibrium evolution of the system (Forbes and Isenberg, 1991; Török and Kliem, 2005; Kliem and Török, 2006; Isenberg and Forbes, 2007), or the onset of a non-ideal instability, often referred to as magnetic reconnection, which abruptly changes the connectivity of the field lines and, in this way, removes or weakens the constraints that would maintain the force balance of a coronal structure. The "tether-cutting" (Moore et al., 2001) and "break-out" (Antiochos et al., 1999) configurations have been the most well-known reconnection geometry, which occurs either below or above the erupting structure, be it a magnetic flux rope or a sheared arcade (Patsourakos et al., 2020).

In the case of major solar eruptive events, the onset of the eruption, either due to ideal or non-ideal instabilities, takes place in the corona, but perturbations propagate along magnetic field lines to reach the lower atmosphere on Alfvénic timescales. In this paper, we focus on dimming and brightening signatures observed at the foot or base of magnetic structures that are undergoing dynamic evolution, such as magnetic reconnection or plasma expansion/eruption. As a direct consequence of magnetic reconnection, energy flux, via particle beams (Fisher et al., 1985), thermal conduction (Longcope, 2014), or Alfvén waves (Fletcher and Hudson, 2008), is transported along newly reconnected field lines to be deposited in the denser lower atmosphere, producing enhanced brightening there. On the other hand, dimming at the base of the corona is primarily an effect of plasma rarefaction due to the expansion of the overlying coronal structures such as a CME, which reduces the pressure of the overlying corona. The expansion or eruption of a coronal structure may occur before or after the onset of magnetic reconnection; therefore, dimming may be observed either before or after brightening in the lower atmosphere.

A solar eruptive event involves a rather complex magnetic configuration, and different parts of the system undergo different dynamics and also interact with each other, such as through reconnection. The spatially resolved, full-disk observations, like those provided by the Solar Dynamics Observatory (SDO; Pesnell et al., 2012), allow us to infer the evolution of different parts of the coronal structures during or before the eruption by examining the behavior at their base in the lower atmosphere. In this paper, we conduct such an experiment on two eruptive flares, using the tempo-spatial sequence of brightening and dimming to reconstruct the evolution of coronal structures in the early phase of their eruption. In the following section, we describe the strategy to identify dimming signatures at the base of the corona (S2). We apply the analysis to observations of an X-class eruptive event SOL20120712, which shows post-eruption dimming (S3), and of a C-class eruptive event SOL20110621, which also exhibits pre-eruption dimming (S4), and use these signatures to infer the properties of the overlying coronal structure. We summarize what is learned from this experiment and discuss the potential to reconstruct the evolution of overlying coronal structures from the brightening and dimming signatures at their base (S5).

2 Tempo-spatial sequence of brightening and dimming

In this paper, we analyze the brightening and dimming signatures in the lower atmosphere of two eruptive events. They exhibit a variety of dimming–brightening sequences that can be used to diagnose the dynamic evolution of overlying coronal structures in the early phase of the eruption.

2.1 Impulsive and prolonged brightening

We identify brightening in the lower atmosphere, as these locations usually map the feet of reconnecting field lines along which energy flux is transported and deposited in the denser lower atmosphere. It has been a well-adopted practice to integrate magnetic flux in these areas of brightening in the lower atmosphere as an estimate of the amount of reconnection flux ψ_{rec} and its time derivative, the reconnection rate $\dot{\psi}_{rec}$ (Fletcher and Hudson, 2001; Asai et al., 2004; Qiu et al., 2004; 2010; Kazachenko et al., 2017). Typically, observations in the optical (such as the H$_{alpha}$ line) and ultraviolet (such as the UV 1,600 Å passband) wavelengths are analyzed to identify brightening signatures. In this study, we analyze either the 1,600 Å or the EUV 304 Å observations from the Atmospheric Imaging Assembly (AIA; Lemen et al., 2012). The contribution to the 1,600 Å broadband emission includes the continuum formed in the temperature minimum region and, in particular, during the flare, optically thin lines like C IV formed at a transition-region temperature of 100,000 K (Simões et al., 2019). The contribution to the EUV 304 Å broadband is more complex, from the upper chromosphere, transition region, and low corona, at a temperature of 0.01–1 MK (O'Dwyer et al., 2010). The EUV 304 Å passband is more sensitive to weak brightening in the upper chromosphere and transition region; on the other hand, structures in the corona, such as filaments, active region loops, and flare loops, are often observed in this passband and are sometimes hard to distinguish from the brightening at the base of the coronal structures.

When magnetic reconnection occurs in the corona, energy flux along newly reconnected field lines travels to the lower atmosphere on Alfvénic timescales and produces a rapid or *impulsive brightening* there. If reconnection forms closed field lines (post-reconnection flare loops), the impulsive energy release in these loops drives chromospheric evaporation, which significantly increases the density (and temperature) of the plasmas trapped in the loops. As a result, *prolonged brightening* is often observed at the base of the post-reconnection flare loops for an extended duration of more than 10 min, before the brightness is attenuated to a pre-flare level, reflecting the timescales of chromospheric evaporation, cooling of the heated corona, and often, continuous gradual heating (Qiu et al., 2013; Qiu and Longcope, 2016). Therefore, light curves similar to those shown in Figure 1A are indicative of reconnection forming closed field lines or flare loops. On the other hand, reconnection leading to open field lines, which do not trap plasmas, would produce only impulsive brightening at its base, as shown in Figure 1B. The pixel light curves are, therefore, indicative of the reconnection geometry.
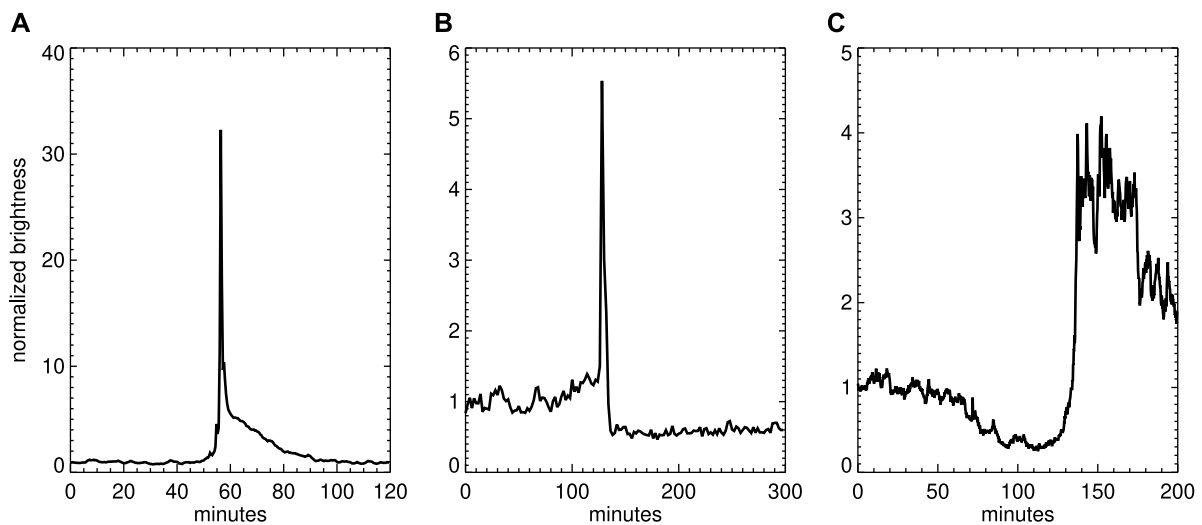
FIGURE 1
Light curves of the brightness in the UV 1,600 or EUV 304 Å passbands in several pixels from various flares observed by the AIA, showing **(A)** impulsive brightening followed by prolonged brightening, **(B)** rapid dimming following impulsive brightening, or **(C)** gradual dimming before brightening.

In this study, we identify brightening pixels in the UV 1,600 Å passband or EUV 304 Å passband when the pixel brightness I is enhanced to be more than N times of its base brightness I_0 for more than τ min; I_0 is the average of the brightness over 20 min during the quiescent (pre-flare) period. N and τ are empirically selected to pick out as many brightening pixels as possible in the lower atmosphere while minimizing the contribution by brightening coronal loops.

2.2 Rapid and gradual dimming

The majority of coronal dimming is observed in the soft X-ray and EUV wavelengths (Sterling and Hudson, 1997; Thompson et al., 1998; Mandrini et al., 2007; Qiu et al., 2007; Temmer et al., 2017; Dissauer et al., 2018; Wang et al., 2019). In this study, we examine signatures in the upper chromosphere, or transition region, where coronal structures undergoing dynamic evolution are anchored. We identify dimming signatures at the base of the corona primarily using observations in the He II 304 passband on the AIA, complemented by analysis of more conventional observations in the EUV passbands, including the EUV 171, 193, and 211 Å passbands. The other EUV passbands are sensitive to temperatures $\geq$ 1 MK (O'Dwyer et al., 2010) of plasmas in the corona. As such, dimming identified in the EUV 304 Å passband tends to occupy smaller areas than those identified in other bands, which often include dimming signatures due to the **removal** or re-orientation of coronal loops along the line of sight (Harvey and Recely, 2002; Harra et al., 2007; Qiu et al., 2007; Downs et al., 2015). In other words, detecting dimming in the transition region lines helps minimize the projection effect.

We examine the time evolution of the brightness at each pixel, normalized to its base brightness. The base brightness is the mean brightness over 20–30 min prior to the eruption. The dimming pixels are identified if the brightness is reduced to $\leq$ 80% of the base brightness continuously for $\geq$10 min. The choice of the minimum

dimming depth at 80% and the minimum dimming duration of 10 min is mostly empirical, justified by the statistical performance of the pixel brightness. For example, the fluctuations in the quiescent brightness of individual pixels are found to be about 10%; therefore, a persistent decrease in the brightness at 20% below the base brightness is considered to reflect genuine dimming.

We assume that these dimming pixels map the feet of the magnetic structures that are expanding or erupting in the corona. Here, we define "expansion" and "eruption" as the global or average bulk motion of the plasma in a magnetic structure, the former referring to motion at subsonic speeds and the latter at super-sonic speeds. If dimming is preceded by brightening at the same or adjacent locations, this is likely an indication that reconnection is opening overlying field lines, and the magnetic flux integrated into the brightening area provides an estimate of the amount of flux removed from above. Furthermore, the dynamic properties, such as the mean speed of the expansion of the overlying corona, can be also estimated from the evolution of the dimming depth.

The pixel light curves given in Figure 1 show various dimming signatures, such as *rapid dimming* following impulsive brightening (b), indicative of reconnection of the opening up of field lines along which plasmas rapidly expand, or *gradual dimming* over tens of minutes, followed by brightening or rapid dimming (panel c), suggesting the quasi-equilibrium expansion of the overlying coronal structure before the onset of reconnection or eruption. The tempo-spatial sequence of dimming and brightening therefore provides clues to the dynamic evolution of the corona.

3 Reconnection-driven post-eruption dimming

An X-class eruptive flare occurred on 12 July 2012 in NOAA-11520. The flare was accompanied by a fast CME with its early-phase motion best captured by STEREO-A (Cheng et al.,
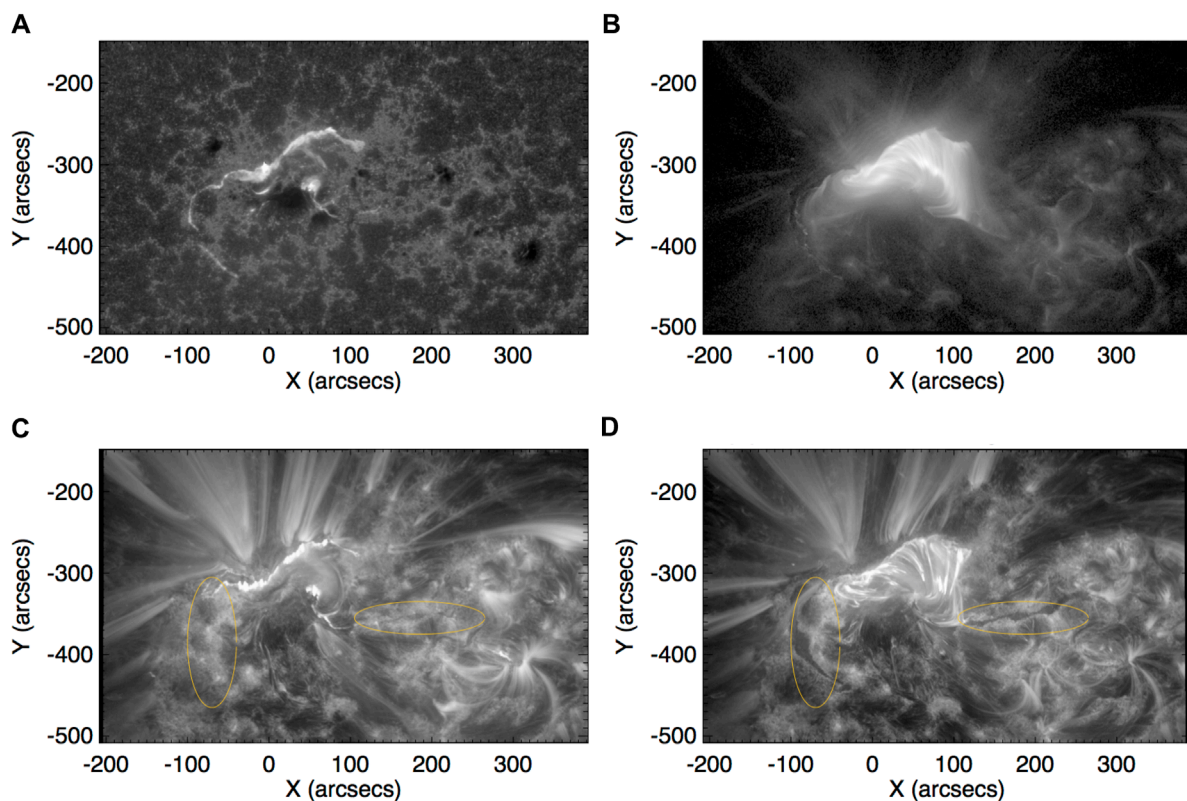
FIGURE 2
Overview of the SOL20120712 eruptive flare observed by the AIA. Top: flare ribbons observed in the UV 1,600 Åpassband **(A)** and flare loops observed in the EUV 131 Åpassband **(B)**. Bottom: flare ribbons and loops observed in the EUV 171 Åpassband at two times **(C,D)**, showing a pair of post-eruption dimming ribbons (their locations indicated by the two orange ovals) extending from the ends of the two flare ribbons. All images are co-aligned to 17:00 UT.

2014; Dudík et al., 2014; Zhu et al., 2020). Figure 2 shows several snapshots of the event observed by the AIA. The eruption occurred in the core active region, forming two bright ribbons in magnetic fields of opposite polarities, outlining the feet of post-reconnection flare loops or closed field lines produced by reconnection. We refer to these two ribbons as *flare ribbons*. Shortly afterward, another set of two long ribbons extended from the flare ribbons in the core region, first briefly brightening and then quickly dimming. We call these two ribbons that became dark *dimming ribbons*, and they were also located in magnetic fields of opposite polarities.

Figure 3A shows, in red, the time sequence of the brightening in the *flare ribbons* in the core region and also the brightening adjacent to the dimming ribbons away from the core region. This reconnection mask is derived using the UV 1,600 Å observations, with the method described by Qiu et al. (2007, 2010). In the same figure, blue indicates the time sequence of the dimming as the brightness is reduced to 80% of the base level (see S2 for identification of the dimming pixels). The dimming (and the preceding brightening) appears to spread rapidly along the dimming ribbons at an apparent speed of more than $100 \, \mathrm{km \, s^{-1}}$, which was noted as a signature of "slipping reconnection" by Dudík et al. (2014).

The magnetic flux integrated in the brightening pixels and in the dimming pixels is measured and shown in Figure 3B, showing that, in this event, the onset of flare reconnection starts at approximately

16 UT, prior to the rapid increase in the dimming. The flare reconnection rate peaks at 16:20 UT and stops at approximately 17 UT, when a total amount of 7×10^{21} Mx has been reconnected. The dimming flux is also measured, which increases quickly after 16:20 UT, and the dimming rate peaks at approximately 17 UT, with the total amount of dimming flux reaching 5×10^{20} Mx encompassed in the dimming ribbons. The associated CME is observed by STEREO; it shows a rapid acceleration starting from 16:10 UT and reaching a maximum at 16:20 UT (Zhu et al., 2020), when the rate of flare reconnection peaks.

The dimming ribbons are most prominently observed in the EUV 304, 171, and 193 Å passbands. Figure 4 shows the time–distance diagrams of the normalized brightness produced along five slits across each *dimming ribbon*; the locations of the slits are indicated by horizontal or vertical bars in Figure 3A. In particular, the diagrams of the 304 Å passband clearly demonstrate dimming after impulsive brightening. Figure 5 shows the epoch plot of the pixel light curves in the two dimming ribbons, or the evolution of the brightness (normalized to the base brightness) with respect to the time of the peak brightness. The figure illustrates the timescales of impulsive brightening, followed by rapid dimming, both within a couple of minutes. In most of these places, dimming does not recover for more than a few hours.

The tempo–spatial sequence of the brightening and dimming in this event suggests the scenario of magnetic reconnection between
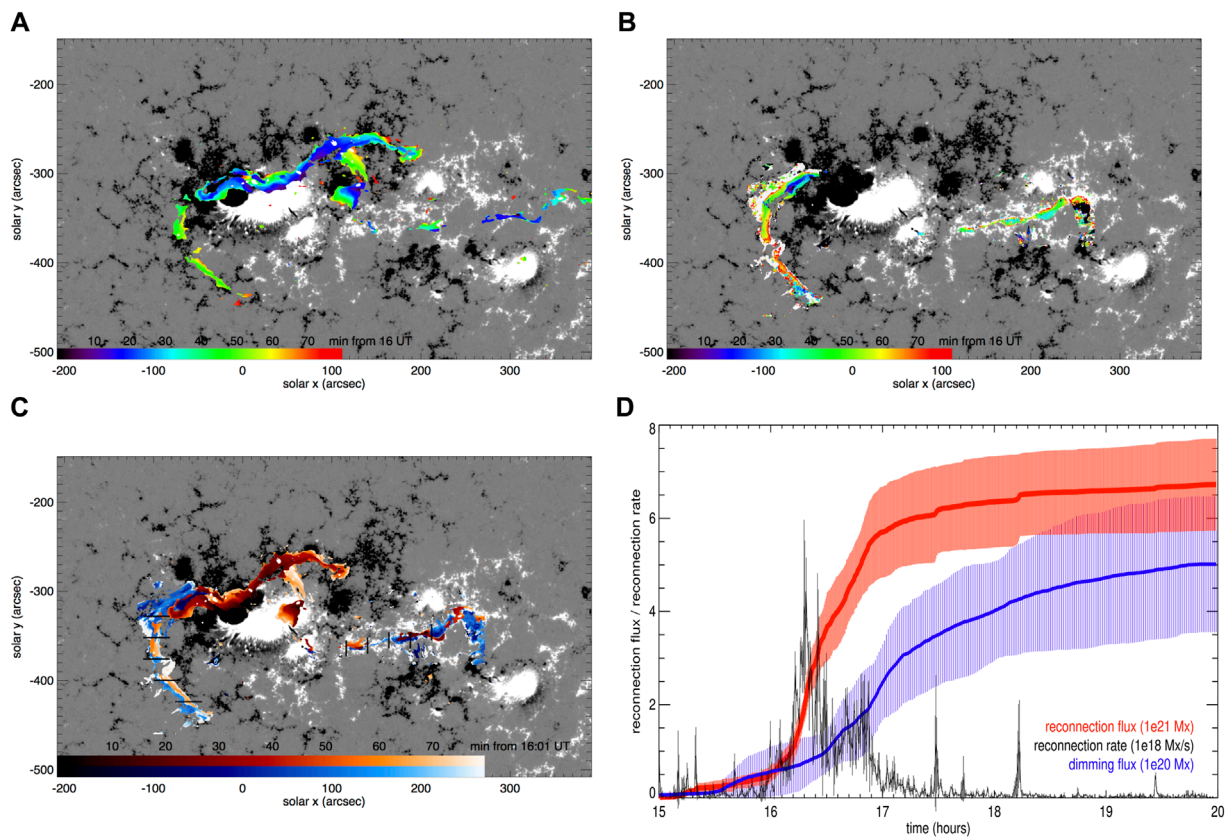
FIGURE 3
Evolution of brightening and dimming. **(A)** Mapping of the brightening evolution (from AIA 1,600 Å) on a photospheric magnetogram (grayscale) of the longitudinal magnetic field component B_{los}. **(B)** Mapping of the dimming evolution (from AIA 304 Å) on the photospheric magnetogram. **(C)** Mapping of brightening (orange) and dimming (blue) on the photospheric magnetogram. **(D)** Reconnection flux ψ_{rec} and reconnection rate $\dot{\psi}_{rec}$ measured from the brightening map and the dimming flux ψ_{dim} measured from the dimming map. In **(A–C)**, the grayscale of the B_{los} map is saturated at ±300 (G). In **(A)** and **(B)**, the rainbow color indicates the onset time of the brightening or the dimming, respectively. In **(C)**, the orange (blue) color scheme indicates the onset time of brightening (dimming) at a given location. It should be noted that in the dimming ribbons, the brightening is covered by the subsequent dimming. The five horizontal bars across the dimming ribbon in the east and the five vertical bars across the dimming ribbon in the west denote the locations of the time–distance diagrams of the normalized brightness in Figure 4.
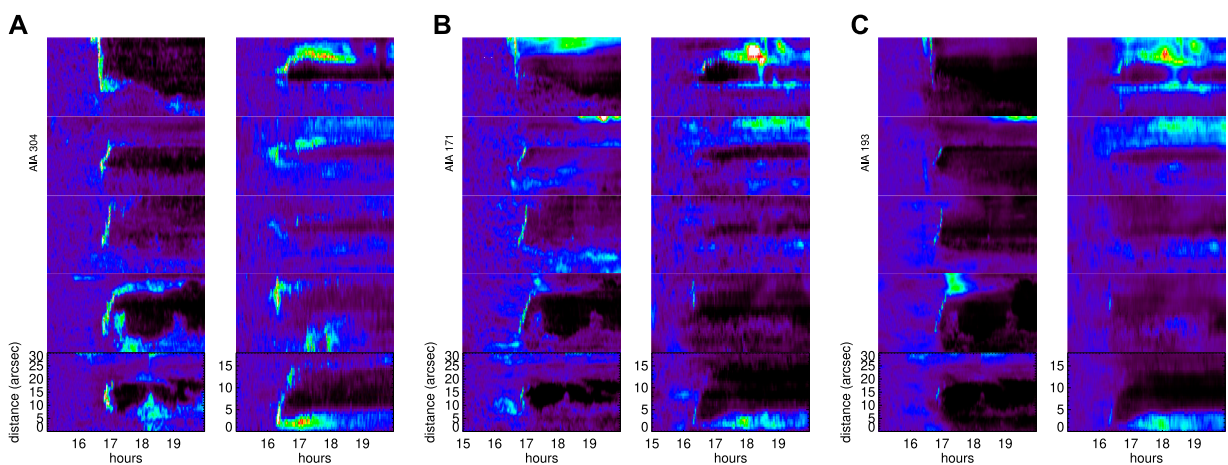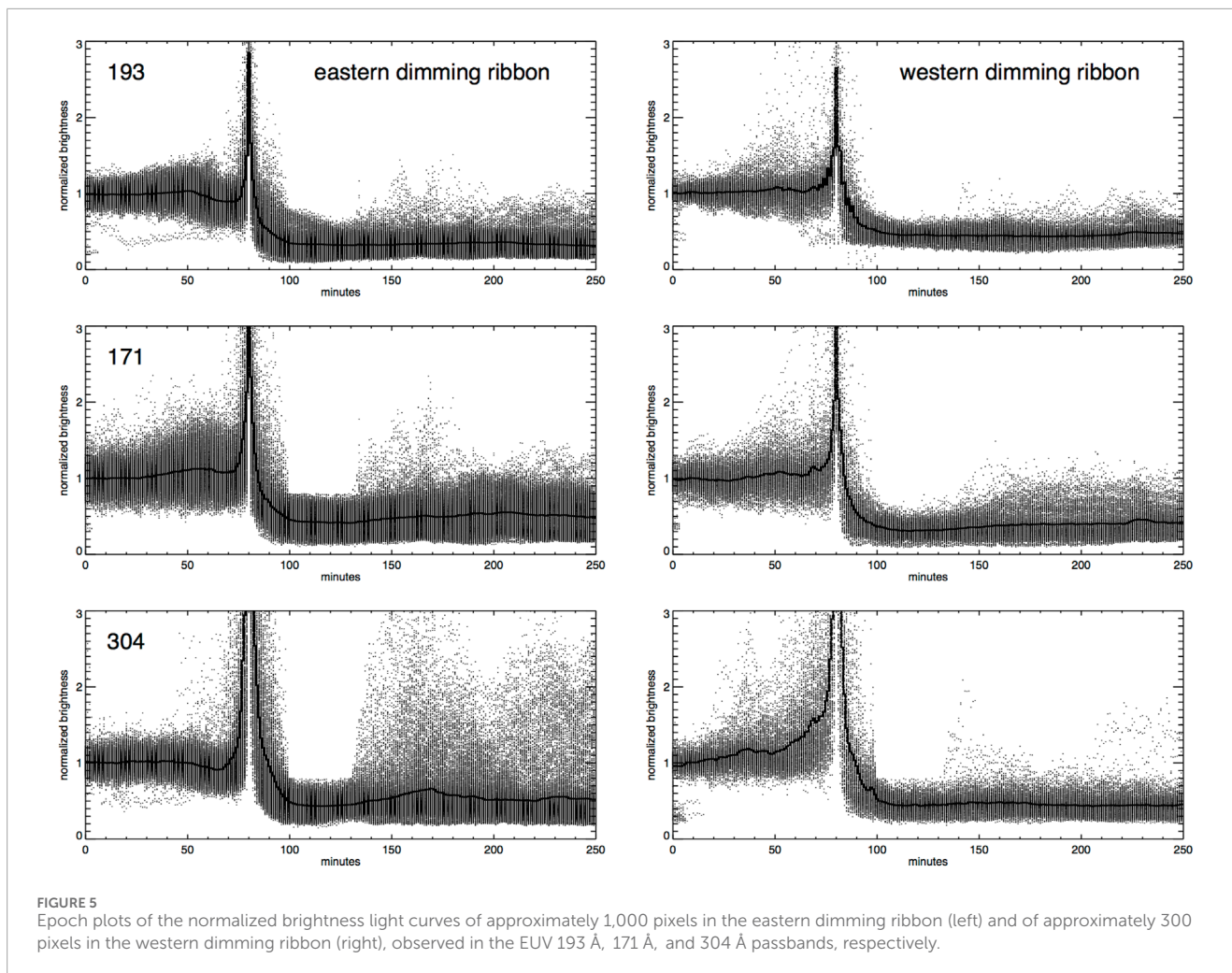

FIGURE 4
Time–distance diagrams of the normalized brightness along the five slits from top to bottom across the dimming ribbon in the east (left) and along the five slits from left to right across the dimming ribbon in the west (right), in the 304 Å **(A)**, 171 Å **(B)**, and 193 Å **(C)** passbands, respectively, all showing rapid dimming after impulsive brightening.

FIGURE 5
Epoch plots of the normalized brightness light curves of approximately 1,000 pixels in the eastern dimming ribbon (left) and of approximately 300 pixels in the western dimming ribbon (right), observed in the EUV 193 Å, 171 Å, and 304 Å passbands, respectively.

an erupting structure from the core region and the overlying arcades or the strapping field. The two dimming ribbons outline the photospheric intersection of separatrices in the complex multi-polar magnetic field where reconnection tends to occur (Dudík et al., 2014). In particular, a potential field extrapolation suggests that the dimming ribbon in the negative magnetic field to the east outlines the feet of an arcade connecting the dimming ribbon to the outer edge of the flare ribbon in the positive magnetic field, and the dimming ribbon in the positive magnetic field to the west maps the feet of another set of arcades with their conjugate feet in the negative magnetic field north of the flare ribbon (Cooper Downs, personal communication). These overlying arcades have to open up for the underlying structure to escape the solar corona.

In summary, in this eruptive event, the dimming analysis does not reveal any significant pre-eruption dynamics of the coronal magnetic structures. Dimming occurs after the onset of flare reconnection in the core region. The pair of dimming ribbons extending outward from the flare ribbons most likely map the feet of several overlying arcades that open up by reconnecting with the erupting structure. In this course, an overlying flux of 5×10^{20} Mx, which is 10% of the flare reconnection flux, is removed from the path of the eruption.

4 Pre-eruption dimming indicative of gradual expansion

A C-class eruptive flare occurred on 21 June 2011. It has been studied by Zhu et al. (2020) and Vievering et al. (2023). The associated CME is best observed by STEREO-A from the limb during its early phase; following the trajectory of the CME, its onset is determined to be at 2:15 UT (Zhu et al., 2020). Figure 6 shows the evolution of the event observed in the EUV 304 Å (left) and 211 Å (right) passbands. A filament is visible prior to the eruption and is erupted around the time of the CME onset. During the eruption, two flare ribbons are brightened as depicted in a standard model; the eruption also causes coronal dimming in a large area to the south of the source region. In this study, we focus on the core region where the eruption originates, attempting to understand the early-phase evolution.

This event exhibits a variety of brightening and dimming signatures different from those of the SOL20120712 event. As shown in Figure 6, prominent dimming signatures are observed in both passbands and, in particular, in the EUV 304 Å base ratio images (middle panels). The dimming primarily occurs in two regions demarcated by the orange boxes that are located at the two ends
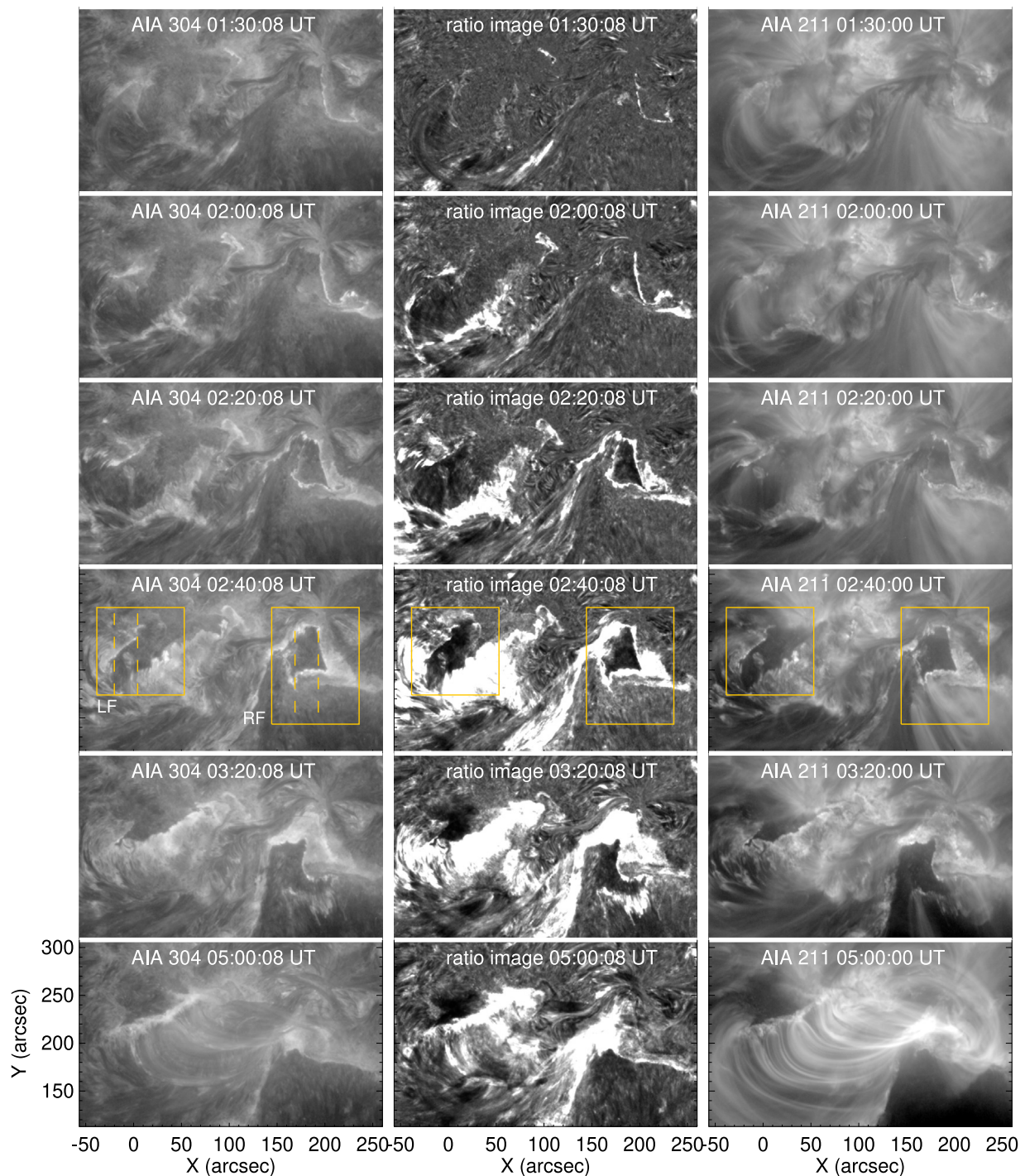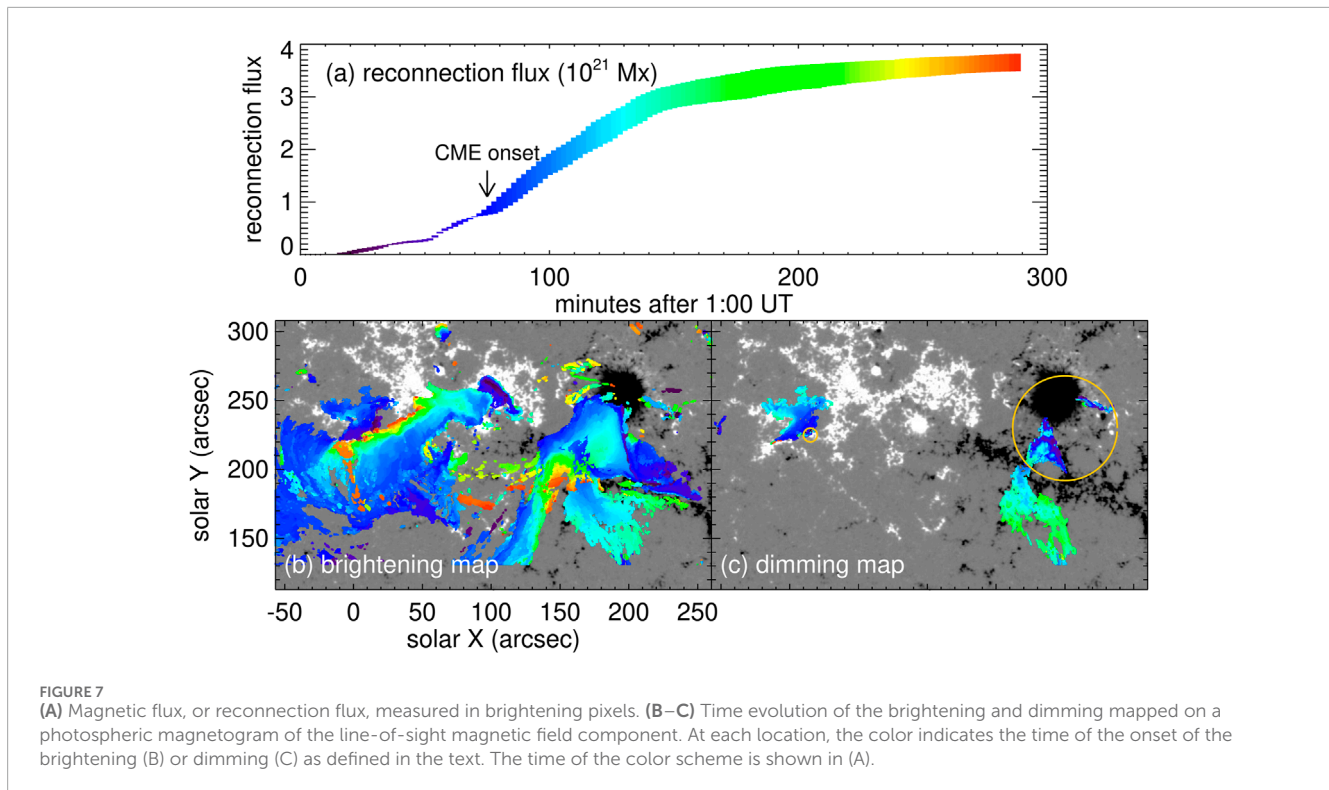
FIGURE 6
Overview of the SOL20110621 eruptive flare observed by the AIA, in the EUV 304 Å passband (left) and 211 Å passband (right). Also shown are base ratio images in the 304 Å passband (middle), with the images normalized to the base image, which is the average of the images from 1:00 UT to 1:20 UT. The two orange boxes denote regions of prominent dimming at the left (LF) and right (RF) feet of a filament visible in the EUV images. The four vertical dashed bars in the left panel mark the slits, along which the time−distance diagrams are produced in Figure 8.

of the filament. The dimming morphology resembles the twin-dimming or core-dimming geometry, similar to the events reported by Webb et al. (2000), Cheng and Qiu (2016), and Wang et al. (2019), suggesting that the twin-dimming regions may map the feet of a flux rope. It is also noted that along the edge of the dimming cores at the

far ends of the two flare ribbons, brightening occurs as early as 1:30 UT, well before the onset of the eruption and flare reconnection that produced the two ribbons.

In this event, the brightening is relatively weak compared with the X-class flare studied in S3; therefore, we use EUV 304 Å passband

FIGURE 7
(A) Magnetic flux, or reconnection flux, measured in brightening pixels. **(B–C)** Time evolution of the brightening and dimming mapped on a photospheric magnetogram of the line-of-sight magnetic field component. At each location, the color indicates the time of the onset of the brightening (B) or dimming (C) as defined in the text. The time of the color scheme is shown in (A).

observations, which are more sensitive to weak brightening than the 1,600 Å passband, to identify brightening signatures at the base of the corona. Two kinds of brightening signatures are observed: flare ribbons underlying closed flare loops exhibit impulsive brightening, followed by a prolonged brightening that gradually decays for over 10 min; on the other hand, several pixels of weak and brief brightening are also identified. Figure 7B shows the timing of brightening[1] superimposed on a photospheric magnetogram of B_{los}. The magnetic flux integrated into the brightening pixels is shown in Figure 7A. It should be noted that due to some mixture of the brightening of coronal features, especially during the filament eruption between 2:15 and 2:40 UT, the measured flux is an overestimate of the reconnection flux ψ_{rec} (see the measurement obtained by Zhu et al. (2020) using 1,600 Å passband images, which likely underestimates the total ψ_{rec}). It is noted that, in this event, the initial brightening occurs adjacent to the twin dimmings at the far ends of the later formed by two flare ribbons, suggesting that pre-eruption reconnection might take place between the hypothetic flux rope and ambient fields. The amount of flux estimated from the early brightening signatures prior to the eruption (2:15 UT) is about one-fifth of the total reconnection flux.

We identify dimming using EUV 304 Å imaging observations following the method outlined in S2. We form the base image as the average of the images between 1:00 and 1:20 UT and define dimming as persistent attenuation at ≤80% of the base brightness I_0 at the same location for more than 10 min. The onset of dimming, which

is shown in Figure 7C, is identified as the time when the brightness starts to decrease below 80% of I_0. The analysis reveals two groups of dimming signatures: one group exhibits gradual dimming over tens of minutes prior to the eruption, and in the other group, dimming occurs after the onset of the eruption (at 2:15 UT), often preceded by impulsive brightening.

Figure 8 shows the time–distance diagrams of the normalized brightness along a few slits shown in Figure 6 and the light curves of a few selected pixels along the slits exhibiting various dimming–brightening sequences similar to those shown in Figure 1. The epoch plots of the two groups of dimming light curves are given in Figure 9, showing the evolution of the pixel brightness with respect to their peak time. The first group exhibits gradual dimming (Figure 9A), with the observed onset of the dimming ranging between 10 and 100 min (average at 54 ± 19 min) before they brightened. The other group of dimming pixels is characterized by rapid dimming following impulsive brightening (Figure 9B), and the peak dimming depth is approximately $42\% \pm 12\%$. In most places, dimming did not recover after more than 3 hours.

The locations of the two groups of dimmings are shown in Figure 7C. The pre-eruption gradual dimmings are within the orange circles; they are mostly clustered in the right region in negative magnetic fields and are bounded by early brightening that outlines a triangle-shaped hook. In the left region in positive magnetic fields, only a small area right next to the flare ribbon exhibits pre-eruption gradual dimming. The post-eruption dimming occupies a larger area in both the left and right feet regions. It appears that, at the onset of the eruption, the pre-eruption dimming spread out into the post-eruption dimming, with a rapid brightening during the transition.

---

1 The onset time of the brightening depends on the empirical threshold used to identify the brightening, and it is typically within 0−3 min of the time of peak brightness.
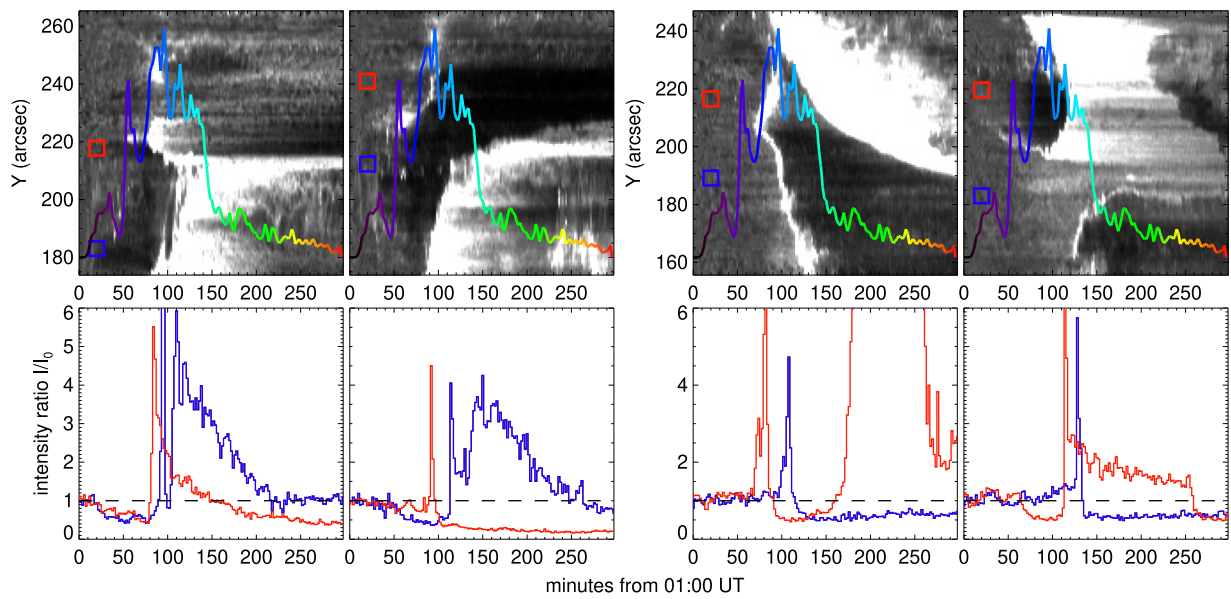
FIGURE 8
Top: time−distance diagrams of the normalized brightness along the four slits shown in Figure 6, two in the left foot region (left) and two in the right foot region (right), superimposed with the reconnection rate $\dot{\psi}_{rec}$. The color code of $\dot{\psi}_{rec}$ is the same as in Figure 7. Bottom: light curves of the normalized brightness at a few locations indicated by the red or blue symbols in the top panels.
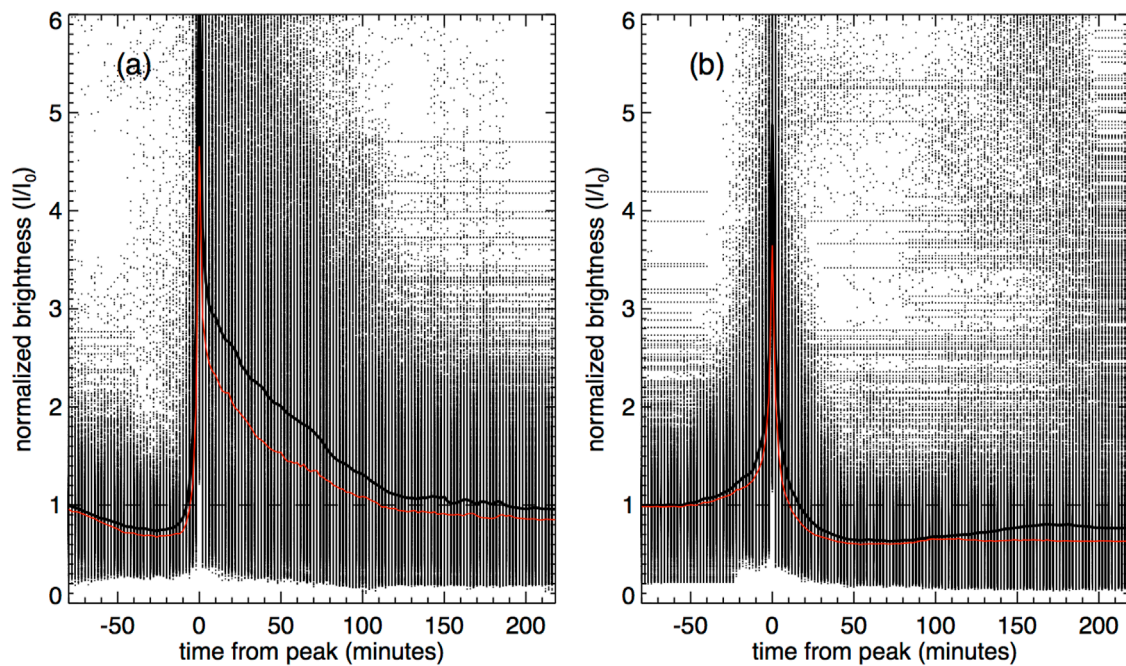

FIGURE 9
Epoch plots of dimming light curves in two groups showing the pre-eruption gradual dimming (left) and the post-eruption impulsive dimming (right). Solid black and red curves indicate the average and median light curves, respectively, of all light curves in a group.

The post-eruption dimming light curves in the second group are similar to those in the SOL20120712 event, suggesting that the erupting structure reconnects with overlying fields and escapes from the corona. However, the geometry of the dimming is different; in this event, the post-eruption dimming appears to map the feet of the

erupting structure that has shifted outward after the onset of the flare reconnection, rather than the feet of overlying arcades. This should be confirmed with future data-driven MHD modeling.

The pre-eruption gradual dimming at the feet of the filament is likely a signature of the quasi-equilibrium expansion of a coronal

structure. We can estimate the mean speed of the expansion from the slope of the dimming depth (Qiu and Cheng, 2017). At the base of the corona, the optically thin transition-region emission can be modeled as the "pressure gauge" (Qiu et al., 2013, and references therein) so that the brightness is proportional to the mean pressure of the overlying corona. As the overlying corona gradually expands, the dimming in terms of the ratio of the brightness to the base brightness, $R \equiv I/I_0$, roughly varies as $\dot{R} \approx \alpha(L_0/L)^{\alpha}(\langle v \rangle/L)$, where $\alpha \geq 1$ is a factor close to unity dependent on the gas expansion model, L is the equivalent height along the line of sight, and L_0 is the height before the expansion. For slow (subsonic) expansion, approximating $L \approx L_0$ and $\alpha \approx 1$, the expansion velocity is roughly $\langle v \rangle \approx \dot{R}L_0$. Fitting the dimming light curves by $R(t) \equiv I(t)/I_0 = R_0 - \dot{R}t$, we derive the dimming slope $\dot{R} \approx 0.001 - 0.01$ min^{-1}, the average being 0.003 min^{-1}, or about 0.3% decrease in brightness per minute. For L_0 of a few tens of Mm, $\langle v \rangle$ is approximately a few kilometers per second. The estimated subsonic expansion speed is consistent with the expansion speed directly observed from limb observations of a different event, which also exhibits persistent gradual dimming, when viewed from the disk, prior to the eruption (Wang et al., 2019).

In summary, the eruptive event SOL20110621 displays different brightening–dimming geometries and sequences from those of the SOL20120712 event. Both pre-eruption and post-eruption dimming occur at the feet of a filament adjacent to flare ribbons, and its geometry resembles the core twin dimming. The twin dimming likely maps the conjugate feet of a coronal structure that gradually expands and then erupts, and this structure carries the total (axial) flux of up to a few times 10^{19} Mx, estimated by integrating the flux in the dimming area. The early brightening surrounding the gradually dimming cores may indicate the coronal structure expanding through (and interacting with) the ambient field.

5 Summary

In this paper, we present an experiment that analyzes the brightening and dimming signatures in the lower atmosphere and uses the tempo-spatial sequence of these signatures to identify overlying magnetic structures that are undergoing dynamic evolution in the early phase of their eruption, such as reconnection or expansion. The experiment is applied to two eruptive events, in which pixel light curves exhibit a variety of brightening–dimming sequences.

For the SOL20120712 event, we did not find signatures indicative of dynamic evolution prior to flare reconnection, which occurs nearly simultaneously with the eruption. The erupting structure then reconnects with the overlying arcades, producing impulsive brightening and rapid dimming at the feet of the arcades as the overlying field lines are opened up and removed from their path. We did not find any signatures likely to map the feet of the erupting structure in this event (e.g., Gou et al., 2023). This is possibly due to the stringent criteria for selecting dimming pixels in this study, which require persistent dimming (for more than 10 min) observed with low-temperature lines characterizing signatures at the base of the corona, such as in the transition region. These requirements are reinforced to help minimize projection

effects and noise fluctuations; on the other hand, dimming at these lines, particularly in the EUV 304 Å passband, is relatively weak. Therefore, dynamic dimming variations on short timescales may not be detected with the method used in this paper, and the estimated dimming flux is likely to be the lower limit.

The SOL20110621 event exhibits gradual pre-eruption dimming at the feet of a filament that erupts later, and the pre-eruption dimming is accompanied by early brightening that outlines the boundary of the gradual dimming at the far ends of flare ribbons formed later. These are likely signatures of the quasi-equilibrium expansion of a coronal structure through the ambient field, which persists for tens of minutes before the explosive loss of equilibrium, leading to eruption. If this structure embodies a pre-existing flux rope, then its gradual expansion and accompanying reconnection with the overlying fields (e.g., Longcope and Forbes, 2014) would bring it to a larger height in favor of the onset of the ideal instabilities, such as the torus instability (Kliem et al., 2014).

Comprehensive modeling (e.g., Rempel et al., 2023) is needed to reconstruct the three-dimensional magnetic configuration and the evolution toward eruption in both events. The identified tempo-spatial sequence of dimming and brightening provides additional observational constraints, or the observed boundary conditions, for the successful modeling of real eruptive events.

Data availability statement

The raw data supporting the conclusion of this article will be made available by the authors, without undue reservation.

Author contributions

JQ: conceptualization, data curation, formal analysis, funding acquisition, investigation, methodology, software, and writing–original draft.

Funding

Conflict of interest

The author declares that the research was conducted in the absence of any commercial or financial relationships that could be construed as a potential conflict of interest.

Publisher's note

All claims expressed in this article are solely those of the authors and do not necessarily represent those of their affiliated organizations, or those of the publisher, the editors, and the reviewers. Any product that may be evaluated in this article, or claim that may be made by its manufacturer, is not guaranteed or endorsed by the publisher.

References

Antiochos, S. K., DeVore, C. R., and Klimchuk, J. A. (1999). A model for solar coronal mass ejections. *ApJ* 510, 485–493. doi:10.1086/306563

Asai, A., Yokoyama, T., Shimojo, M., Masuda, S., Kurokawa, H., and Shibata, K. (2004). Flare ribbon expansion and energy release rate. *ApJ* 611, 557–567. doi:10.1086/422159

Cheng, J. X., and Qiu, J. (2016). *ApJ* 825, 37. doi:10.3847/0004-637X/825/1/37

Cheng, X., Ding, M. D., Zhang, J., Sun, X. D., Guo, Y., Wang, Y. M., et al. (2014). *ApJ* 789, 93. doi:10.1088/0004-637X/789/2/93

Cranmer, S. R. (2009). Coronal holes. *Living Rev. Sol. Phys.* 6, 3. doi:10.12942/lrsp-2009-3

Dissauer, K., Veronig, A. M., Temmer, M., Podladchikova, T., and Vanninathan, K. (2018). On the detection of coronal dimmings and the extraction of their characteristic properties. *ApJ* 855, 137. doi:10.3847/1538-4357/aaadb5

Downs, C., Török, T., Titov, V., Liu, W., Linker, J., and Mikic, Z. (2015). *AAS/AGU triennial earth-sun summit*, 1. Indianapolis, IN: AAS/AGU Triennial Earth-Sun Summit. 304.01.

Dudík, J., Janvier, M., Aulanier, G., Del Zanna, G., Karlický, M., Mason, H. E., et al. (2014). SLIPPING MAGNETIC RECONNECTION DURING AN X-CLASS SOLAR FLARE OBSERVED BY *SDO*/AIA. *ApJ* 784, 144. doi:10.1088/0004-637X/784/2/144

Fisher, G. H., Canfield, R. C., and McClymont, A. N. (1985). Flare loop radiative hydrodynamics - Part Six - chromospheric evaporation due to heating by nonthermal electrons. *ApJ* 289, 425. doi:10.1086/162902

Fletcher, L., and Hudson, H. (2001). *SoPh* 204, 69–89. doi:10.1023/A:1014275821318

Fletcher, L., and Hudson, H. S. (2008). Impulsive phase flare energy transport by large-scale Alfvén waves and the electron acceleration problem. *ApJ* 675, 1645–1655. doi:10.1086/527044

Forbes, T. G., and Isenberg, P. A. (1991). A catastrophe mechanism for coronal mass ejections. *ApJ* 373, 294. doi:10.1086/170051

Gou, T., Liu, R., Veronig, A. M., Zhuang, B., Li, T., Wang, W., et al. (2023). Complete replacement of magnetic flux in a flux rope during a coronal mass ejection. *Nat. Astron.* 7, 815–824. doi:10.1038/s41550-023-01966-2

Harra, L. K., Hara, H., Imada, S., Young, P., Williams, D. R., Sterling, A. C., et al. (2007). *PASJ* 59–S801. doi:10.1093/pasj/59.sp3.S801

Harvey, K. L., and Recely, F. (2002). *SoPh* 211, 31–52. doi:10.1023/A:1022469023581

Isenberg, P. A., and Forbes, T. G. (2007). A three-dimensional line-tied magnetic field model for solar eruptions. *ApJ* 670, 1453–1466. doi:10.1086/522025

Kazachenko, M. D., Lynch, B. J., Welsch, B. T., and Sun, X. (2017). A database of flare ribbon properties from the solar dynamics observatory. I. Reconnection flux. *ApJ* 845, 49. doi:10.3847/1538-4357/aa7ed6

Kliem, B., Lin, J., Forbes, T. G., Priest, E. R., and Török, T. (2014). *ApJ* 789, 46. doi:10.1088/0004-637X/789/1/46

Kliem, B., and Török, T. (2006). Torus instability. *PhRvL* 96, 255002. doi:10.1103/PhysRevLett.96.255002

Lemen, J. R., Title, A. M., Akin, D. J., Boerner, P. F., Chou, C., Drake, J. F., et al. (2012). The atmospheric imaging assembly (AIA) on the solar dynamics observatory (SDO). *SoPh* 275, 17–40. doi:10.1007/s11207-011-9776-8

Longcope, D. W. (2014). *ApJ* 795, 10. doi:10.1088/0004-637X/795/1/10

Longcope, D. W., and Forbes, T. G. (2014). Breakout and tether-cutting eruption models are both catastrophic (sometimes). *SoPh* 289, 2091–2122. doi:10.1007/s11207-013-0464-8

Lowder, C., Qiu, J., and Leamon, R. (2017). Coronal holes and open magnetic flux over cycles 23 and 24. *SoPh* 292, 18. doi:10.1007/s11207-016-1041-8

Mandrini, C. H., Nakwacki, M. S., Attrill, G., van Driel-Gesztelyi, L., Démoulin, P., Dasso, S., et al. (2007). *SoPh* 244, 25–43. doi:10.1007/s11207-007-9020-8

Moore, R. L., Sterling, A. C., Hudson, H. S., and Lemen, J. R. (2001). Onset of the magnetic explosion in solar flares and coronal mass ejections. *ApJ* 552, 833–848. doi:10.1086/320559

O'Dwyer, B., Del Zanna, G., Mason, H. E., Weber, M. A., and Tripathi, D. (2010). SDO/AIA response to coronal hole, quiet Sun, active region, and flare plasma. *A&A* 521, A21. doi:10.1051/0004-6361/201014872

Patsourakos, S., Vourlidas, A., Török, T., Kliem, B., Antiochos, S. K., Archontis, V., et al. (2020). Decoding the pre-eruptive magnetic field configurations of coronal mass ejections. *SSRv* 216, 131. doi:10.1007/s11214-020-00757-9

Pesnell, W. D., Thompson, B. J., and Chamberlin, P. C. (2012). The solar dynamics observatory (SDO). *SoPh* 275, 3–15. doi:10.1007/s11207-011-9841-3

Qiu, J., and Cheng, J. (2017). Gradual solar coronal dimming and evolution of coronal mass ejection in the early phase. *ApJL* 838, L6. doi:10.3847/2041-8213/aa6798

Qiu, J., Hu, Q., Howard, T. A., and Yurchyshyn, V. B. (2007). On the magnetic flux budget in low-corona magnetic reconnection and interplanetary coronal mass ejections. *ApJ* 659, 758–772. doi:10.1086/512060

Qiu, J., Liu, W., Hill, N., and Kazachenko, M. (2010). *ApJ* 725, 319–330. doi:10.1088/0004-637X/725/1/319

Qiu, J., and Longcope, D. W. (2016). *ApJ* 820, 14. doi:10.3847/0004-637X/820/1/14

Qiu, J., Sturrock, Z., Longcope, D. W., Klimchuk, J. A., and Liu, W.-J. (2013). *ApJ* 774, 14. doi:10.1088/0004-637X/774/1/14

Qiu, J., Wang, H., Cheng, C. Z., and Gary, D. E. (2004). Magnetic reconnection and mass acceleration in flare–coronal mass ejection events. *ApJ* 604, 900–905. doi:10.1086/382122

Rempel, M., Chintzoglou, G., Cheung, M. C. M., Fan, Y., and Kleint, L. (2023). Comprehensive radiative MHD simulations of eruptive flares above collisional polarity inversion lines. *ApJ* 955, 105. doi:10.3847/1538-4357/aced4d

Simões, P. J. A., Reid, H. A. S., Milligan, R. O., and Fletcher, L. (2019). The spectral content of SDO/AIA 1600 and 1700 Å filters from flare and plage observations. *ApJ* 870, 114. doi:10.3847/1538-4357/aaf28d

Sterling, A. C., and Hudson, H. S. (1997). [ITAL]Yohkoh[/ITAL] SXT observations of X-ray "dimming" associated with a halo coronal mass ejection. *ApJL* 491, L55–L58. doi:10.1086/311043

Temmer, M., Thalmann, J. K., Dissauer, K., Veronig, A. M., Tschernitz, J., Hinterreiter, J., et al. (2017). On flare-CME characteristics from sun to earth combining remote-sensing image data with *in situ* measurements supported by modeling. *SoPh* 292, 93. doi:10.1007/s11207-017-1112-5

Thompson, B. J., Plunkett, S. P., Gurman, J. B., Newmark, J. S., St. Cyr, O. C., and Michels, D. J. (1998). *SOHO*/EIT observations of an Earth-directed coronal mass ejection on May 12, 1997. *Geophys. Res. Lett.* 25, 2465–2468. doi:10.1029/98GL50429

Thompson, B. J., Qiu, J., Lugaz, N., and Webb, D. F. (2021). "Solar flares and coronal mass ejections," in *Solar physics and solar wind*. Editors N. E. Raouafi, and A. Vourlidas, 1, 179–220. doi:10.1002/9781119815600.ch5

Török, T., and Kliem, B. (2005). Confined and ejective eruptions of kink-unstable flux ropes. *ApJL* 630, L97–L100. doi:10.1086/462412

Vievering, J. T., Vourlidas, A., Zhu, C., Qiu, J., and Glesener, L. (2023). Evolution of solar eruptive events: investigating the relationships among magnetic reconnection, flare energy release, and coronal mass ejections. *ApJ* 946, 81. doi:10.3847/1538-4357/acbe3d

Wang, W., Zhu, C., Qiu, J., Liu, R., Yang, K. E., and Hu, Q. (2019). Evolution of a magnetic flux rope toward eruption. *ApJ* 871, 25. doi:10.3847/1538-4357/aaf3ba

Webb, D. F., Lepping, R. P., Burlaga, L. F., DeForest, C. E., Larson, D. E., Martin, S. F., et al. (2000). The origin and development of the May 1997 magnetic cloud. *J. Geophys. Res.* 105, 27251–27259. doi:10.1029/2000JA000021

Zhu, C., Qiu, J., Liewer, P., Vourlidas, A., Spiegel, M., and Hu, Q. (2020). *ApJ* 893, 141. doi:10.3847/1538-4357/ab838a